Bioactive Materials 49 (2025) 207–217

Contents lists available at ScienceDirect

Bioactive Materials

journal homepage: www.keaipublishing.com/en/journals/bioactive-materials

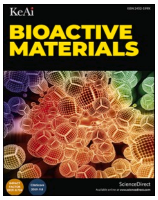

Engineering a stem cell-embedded bilayer hydrogel with biomimetic collagen mineralization for tendon-bone interface healing

Tingyun Lei [a,c,1], Tao Zhang [a,1], Tianshun Fang [d,1], Jie Han [d,1], Chunyi Gu [e], Youguo Liao [f], Yang Fei [a,c], Junchao Luo [a,d], Huanhuan Liu [g,h], Yan Wu [a], Weiliang Shen [a,c,*], Xiao Chen [a,**], Zi Yin [b,i,***], Junjuan Wang [e,****]

[a] *Department of Sports Medicine & Orthopedic Surgery, The Second Affiliated Hospital, Zhejiang University School of Medicine, Hangzhou, Zhejiang Province, China*
[b] *Department of Orthopedic Surgery of Sir Run Run Shaw Hospital & Liangzhu Laboratory, Zhejiang University School of Medicine, Hangzhou, China*
[c] *Binjiang Institute of Zhejiang University, Hangzhou, Zhejiang Province, China*
[d] *Dr. Li Dak Sum & Yip Yio Chin Center for Stem Cells and Regenerative Medicine, Zhejiang University School of Medicine, Hangzhou, China*
[e] *School of Basic Medical Sciences and Forensic Medicine, Hangzhou Medical College, Hangzhou, Zhejiang Province, China*
[f] *Department of Burns and Wound Care Center, The Second Affiliated Hospital, Zhejiang University School of Medicine, Hangzhou, China*
[g] *Ohio Musculoskeletal and Neurological Institute (OMNI), Ohio University, Athens, OH, USA*
[h] *Department of Biomedical Sciences, Ohio University Heritage College of Osteopathic Medicine, Ohio University, Athens, OH, USA*
[i] *Institute of Cell Biology, Zhejiang University, Hangzhou, China*

ARTICLE INFO

Keywords:
Tendon-bone interface
Tendon stem cell
Biomimetic mineralization
Hydrogel

ABSTRACT

The tendon-bone interface effectively transfers mechanical stress for movement, yet its regeneration presents significant clinical challenges due to its hierarchical structure and composition. Biomimetic strategies that replicate the distinctive characteristics have demonstrated potential for enhancing the healing process. However, there remains a challenge in developing a composite that replicates the nanostructure of the tendon-bone interface and embeds living cells. Here, we engineered a nanoscale biomimetic bilayer hydrogel embedded with tendon stem cells for tendon-bone interface healing. Specifically, the biomimetic hydrogel incorporates intra- and extrafibrillar mineralized collagen fibrils as well as non-mineralized collagen fibrils resembling the tendon-bone interface at the nanoscale. Furthermore, biomimetic mineralization with the presence of cells realizes living tendon-bone-like tissue constructs. In the *in vivo* patella-patellar tendon-interface injury model, the tendon stem cell-laden biomimetic hydrogel promoted tendon-bone interface regeneration, demonstrated by increased fibrocartilage formation, improved motor function, and enhanced biomechanical outcomes. This study highlights the potential of the stem cell-laden biomimetic hydrogel as an effective strategy for tendon-bone interface regeneration, offering a novel approach to engineering complex tissue interfaces.

1. Introduction

The tendon-bone interface, a critical junction where tendon inserts into the bone, plays a pivotal role in the transmission of mechanical stress essential for motor functions [1]. It is composed of tendon, non-mineralized fibrocartilage, mineralized fibrocartilage and bone, displaying gradients in tissue organization, composition, and mechanical properties [2]. In recent years, as the population ages and the culture of fitness-related activities expands, the incidence of tendon-bone injuries has become more prevalent, leading to pain, sleep disturbances,

---

Peer review under the responsibility of KeAi Communications Co., Ltd.

* Corresponding authors. Department of Sports Medicine & Orthopedic Surgery, The Second Affiliated Hospital, Zhejiang University School of Medicine, Hangzhou, Zhejiang Province, China.

** Corresponding author.

*** Corresponding author. Department of Orthopedic Surgery of Sir Run Run Shaw Hospital & Liangzhu Laboratory, Zhejiang University School of Medicine, Hangzhou, China.

**** Corresponding author.

E-mail addresses: wlshen@zju.edu.cn (W. Shen), chenxiao-610@zju.edu.cn (X. Chen), yinzi@zju.edu.cn (Z. Yin), wang.junjuan@foxmail.com (J. Wang).

[1] These authors contributed equally.

https://doi.org/10.1016/j.bioactmat.2025.03.001
Received 6 October 2024; Received in revised form 21 February 2025; Accepted 1 March 2025

limited motion, and dysfunction [3]. The regeneration of fibrocartilage is crucial for restoration of the biomechanical properties at the tendon-bone interface function [4]. However, the clinical reconstruction of the tendon-bone interface often fails to recapitulate the organized structure of the native fibrocartilage and tends to form scar tissues, the inferior mechanics of which lead to a high incidence of retears (26%–94 %) [5].

Biomimetic strategies have attracted considerable interest in the field of complex tissue regeneration, owing to their capacity to address the various physiological needs of different tissue types. Biomimetic scaffolds made from synthetic, natural, and inorganic materials have been engineered to emulate the native gradient structure and composition of the tendon-bone interface [6]. Despite significant strides, current biomimetic scaffolds mimic the microscale features of native tendon-bone transition zone, but do not fully reconstruct the natural ultrastructure. A successful biomimetic strategy for interface regeneration requires a deep understanding of the structure and composition of the native tissue. As known, bone is hierarchically organized through cross-fibrillar mineralized collagen fibrils [7]. Our previous study revealed that the collagen fibrils in mineralized fibrocartilage undergo partial mineralization, forming a continuous cross-fibrillar mineral phase [8]. These findings, corroborated by the observations of Buss et al., highlight the presence of a crossfibrillar mineral tessellation pattern similar to that found in lamellar bone [9]. Highly aligned collage fibrils are the most abundant component of the tendon [10]. Thus, non-mineralized and mineralized collagen fibrils are the building blocks for the fabrication of high-precision biomimetic scaffolds.

Collagen mineralization is an essential biological process in many skeletal elements, such as bone and dentin. The precursor phase for bone formation is amorphous calcium phosphate (ACP) rather than hydroxyapatite (HAP) [11–13]. Collagen molecules self-assemble into collagen fibrils, with channels in the collagen fibrils' a- and e-bands facilitating ACP infiltration [14]. ACP can penetrate collagen fibrils and subsequently transform into HAP crystals and propagate within and along collagen fibrils [15]. The intrafibrillar deposition of apatite crystals is believed to be synergistically coordinated by matrix non-collagenous proteins (NCPs) [16]. To mimic the mineralized collagen fibrils, polyelectrolytes, including polyaspartic acid (pAsp) and polyacrylic acid, are utilized as analogs to NCPs and have demonstrated the ability to guide the intrafibrillar mineralization of collagen fibrils *in vitro* [17]. Therefore, a biomimetic mineralization strategy holds promise for developing high-precision tendon-bone scaffolds.

Cells are the key participants in tissue regeneration. Scaffolds post-seeded with cells *in vitro* oversimplify the native 3D microenvironment found *in vivo*. Stem cells within a 3D culture system display cellular behaviors that more closely replicate the patterns observed when they are *in vivo*, including cell adhesion, viability, self-renewal capacity, migratory activity, and differentiation potential [18]. Accordingly, embedding cells within a collagen hydrogel and employing biomimetic mineralization could provide a 3D nanoscale biomimetic microenvironment conducive to cellular function [19]. Additionally, the selection of appropriate seed cells is essential for tissue regeneration. Compared to the commonly used bone marrow stem cells (BMSCs) and adipose-derived stem cells, tendon stem/progenitor cells (TSPCs) have shown remarkable potential for tendon-bone interface repair, exhibiting osteogenic and tenogenic capabilities, and the potential to differentiate into fibrochondrocytes [4,20]. A previous lineage tracing study suggested that enthesis fibrocartilage likely originates from the tendon [21], highlighting TSPCs as attractive candidates for fibrocartilage regeneration.

This study introduces a novel cell-laden biomimetic hydrogel that resembles the nanostructure of the native tendon-bone interface. By integrating TSPCs within biomimetic hydrogel, we aim to promote the function and structural recovery of the tendon-bone interface, providing new strategies for interface regeneration.

2. Methods

2.1. Collagen hydrogel preparation

Collagen was extracted from porcine tendons. To prepare the collagen hydrogel, acid solubilized collagen was mixed with 10 × PBS (Gibco) and DMEM/F12 (Gibco) on ice, and the pH of the mixture was adjusted to 7.4 using 1 M NaOH. The final concentration of collagen was 10 mg/mL. Subsequently, the hydrogel precursor was placed in a 5 % CO_2 incubator at 37 °C for 30 min to facilitate self-assembly. For the cell-laden collagen hydrogel, DMEM/F12 containing cells were used and the mixture was mixed thoroughly to ensure uniform distribution of cells within the hydrogel. The other steps were as described above.

2.2. Cell isolation and culture

Tail tendon samples were harvested from Sprague-Dawley rats, dissected into fine fragments, and enzymatic digestion with 0.2 % collagenase type I. Single cell suspensions were then cultured in DMEM/F12 (Gibco) supplemented with 1 % penicillin-streptomycin (PS, Gibco) and 10 % fetal bovine serum (FBS, Gibco).

2.3. Collagen hydrogel mineralization

To prepare the mineralization medium, 3.34 mM $CaCl_2$ and 19 mM Na_2HPO_4 in DMEM/F12 supplemented with 10 % FBS and 1 % PS were mixed in equal volumes. DMEM/F12 containing polyaspartic acid (pAsp) (10 mg/mL) was added to the $CaCl_2$-containing medium before the addition of the Na_2HPO_4-containing medium. The final mineralization medium contained 1.67 mM $CaCl_2$, 240 μg/mL pAsp, and 9.5 mM Na_2HPO_4. Genipin (MedChemExpress) was added to the mineralization medium at a concentration of 0.15 mM. The collagen hydrogels were incubated with the mineralization medium for 3 days to induce mineralization, during which the medium was refreshed every day.

2.4. Thermogravimetric analysis

Thermogravimetric analysis was conducted with Mettler Toledo STARe System TGA2 (Mettler Toledo Corp.). Prior to analysis, the samples underwent drying were dried at 37 °C for a period of 3 consecutive days. Subsequently, the samples were heated under an air condition from room temperature to 800 °C. The mass recorded at 660 °C was considered as the total inorganic mass.

2.5. Fourier transform infrared spectroscopy analysis (FTIR)

FTIR analysis was performed using a NICOLET iS50FT-IR spectrometer (Thermo Scientific). The spectra were acquired with 32 scans at a resolution of 4 cm^{-1} ranging from 4000^{-1} to 400 cm^{-1}.

2.6. Transmission electron microscopy (TEM)

Mineralized and non-mineralized hydrogels were chopped and immersed in ice-cold 0.1 M ammonium bicarbonate. The minced hydrogels were processed using a tissue homogenizer at a frequency of 65Hz until no visible fragments remained. The resulting homogenate was carefully pipetted onto carbon-coated TEM grids and air dried. The non-mineralized samples were stained with uranyl acetate. Subsequently, all samples were examined using TEM (JEM).

2.7. Scanning electron microscopy (SEM)

Mineralized and non-mineralized hydrogels were fixed using 2.5 % glutaraldehyde for 1 h at room temperature, after which they were thoroughly rinsed with distilled water. The samples then underwent a graded series of ethanol dehydration steps, each lasting 10 min.

Following dehydration, the samples were critical point dried, sputter coated with Au-palladium, and observed using SEM Nova Nano 450 (Thermo FEI). Elemental analysis of the samples was performed using EDX detector.

2.8. *Cryo-scanning electron microscopy (cryo-SEM)*

Quickly freeze the samples in liquid ethane, and then transfer them from the liquid nitrogen bath to a vacuum chamber. Sublimate the frozen samples for 10 min at −90 °C. After sublimation, sputter-coat the frozen samples with a platinum layer to enhance their conductivity. Transfer the samples to the Cryo-SEM stage and image them using an accelerating voltage of 2 kV (Thermo Fisher Scientific).

2.9. *Nanoindentation*

The specimens were immersed in a PBS solution and then subjected to indentation testing using a conical diamond probe with a curvature radius of 48.5 μm. The indentation was force-controlled to achieve a maximum indentation depth of 1000 nm. The test included loading, holding, and unloading stages, during which the displacement (h) of the indenter and the applied load (P) were recorded. The recorded data were analyzed to determine the elastic modulus of the tested samples.

2.10. *Stochastic optical reconstruction microscopy (STORM) imaging*

The mineralized hydrogel was incubated with collagen I antibody (abcam) overnight at 4 °C. Then, the sample was labeled with secondary antibody and calcein (Aladdin). Data was obtained by Nikon Ti-E inverted optical microscope and analyzed with Nikon NIS-Elements AR.

2.11. *Cell viability*

Cell viability was evaluated using the Calcein-AM/PI Double Stain Kit (Yeasen Biotechnology). The assessment was conducted at 1, 4, and 7 days post-seeding in accordance with the protocol provided by the manufacturer.

2.12. *Cell morphology*

The samples were fixed with 4 % paraformaldehyde and permeabilized with Triton X-100. Then, the samples were stained with Phalloidin-iFluor 488 (abcam) and 4′,6-diamidino-2-phenylindole (DAPI). Fluorescent images were captured using confocal microscope (Olympus). The sample preparation for SEM was as described above.

2.13. *RNA-sequencing (RNA-seq)*

For bulk RNA-seq analysis, the cell-laden hydrogels were cultured in either mineralization or growth medium for 3 days. Total RNA was extracted from the hydrogels with an RNA-Quick Purification Kit (ES Science). After confirming RNA quality, reverse transcription was carried out to generate DNA libraries for subsequent sequencing. The genome sequencing was performed by Personal Biotechnology Company (Shanghai, China) by using the Illumina Novaseq platform. The differentially expressed genes (DEG) were calculated using DESeq2.

2.14. *Surgical procedure*

The study protocol was ethically approved by the Institutional Animal Care and Use Committee of Zhejiang University (ZJU20230256). SD rats were randomly assigned into four groups: blank control (BC), non-mineralized collagen hydrogel (NMCH), bilayer biomimetic mineralized collagen hydrogel (BMCH), and bilayer biomimetic mineralized collagen hydrogel-tendon stem/progenitor cell (BMCH-TSPC). The BMCH and BMCH-TSPC samples are bilayer including non-mineralized and mineralized layer. The preparation of hydrogel was as described above. Cell concentration of BMCH-TSPC was 3×10^6 cells/mL. Under general anesthesia, a fenestration model was created at the interface of patellar-tendon. The dimensions of the fenestration were precisely 1.5 mm in width and 4 mm in length, encompassing the distal 2 mm of the patella, including its connected fibrocartilage layer, as well as an additional 2 mm of the patellar tendon. Following this, NMCH, BMCH and BMCH-TSPC grafts were placed within the defect site. The rats were euthanized after 2 and 4 weeks, and specimens of the quadriceps-patella-patellar tendon-tibia complex were collected for further analysis.

2.15. *Mechanical testing*

Mechanical properties were evaluated using a tension/compression system (Instron). The hind limbs of the rats were harvested and the soft tissues surrounding the knee were removed. The quadriceps-patella-patellar tendon-tibia complex was then securely fixed to a custom-made clamp. An initial preload of 0.1 N was applied to pretreat each sample with a cyclic elongation of 0–0.5 mm for 5 cycles at a speed of 5 mm/min. Subsequently, load-to-failure tests were performed with an elongation speed of 5 mm/min to determine the mechanical properties of the tissue. The structural properties were quantified by several parameters including stiffness (N/mm), Young's modulus (MPa), failure force (N), and stress at failure (MPa).

2.16. *Running testing*

Rats were tested on a treadmill with an acceleration of 2 m/min^2, and the running distance within 10 min was recorded.

2.17. *Micro-computed tomography (Micro-CT) imaging and analysis*

The samples were fixed with 4 % paraformaldehyde and subjected to analysis using micro-CT (Milabs). The subsequent reconstruction and quantitative analysis were conducted using Imalytics Preclinical software.

2.18. *Histology and immunofluorescence staining*

The specimens were fixed in 4 % paraformaldehyde, followed by decalcification with a 10 % ethylene diamine tetra-acetic acid solution. The specimens were then subjected to a series of graded ethanol solutions for dehydration, and embedded in paraffin. The embedded samples were sectioned at a thickness of 5 μm for histological examination. Hematoxylin & eosin (H&E), Safranin O-Fast Green (SO-FG), Masson, and toluidine blue (TB) staining were performed to assess tissue morphology and matrix deposition.

For immunofluorescent staining, the sections underwent a series of procedure including deparaffinization, hydration, antigen retrieval, and antibody incubation with specific antibodies as follows: COL2A1 (Proteintech) and SOX9 (Abcam). Fluorescent images were captured using confocal microscope (Olympus).

2.19. *Single cell preparation and sequencing*

At 2 weeks post-surgery, patella-patellar tendon specimens were carefully extracted from the rats and rinsed with PBS. The tissues were finely minced and subsequently subjected to enzymatic digestion (0.3 % collagenase I (Gibco), 0.2 % collagenase II (Gibco), and 0.4 % Dispase (Roche)) at 37 °C for 2 h. The digested tissue was filtered through a 40 μm strain. Single cell RNA sequencing (scRNA-seq) libraries were constructed using the GEXSCOPE® Single Cell RNA Library Kits and were subjected to further sequencing.

2.20. scRNA-seq data analysis

The raw data were subjected by CeleScope (Singleron Biotechnologies) to obtain the gene expression matrix. Seurat was used for dimension reduction and clustering. For quality control, cells with expression levels of less than 200 genes and over 5000 genes, mitochondrial genes over 20 % and erythrocyte genes over 10 % were removed. Then, data normalization, identification of highly variable features, data scaling, dimensional reduction, and unsupervised clustering were performed. Differentially expressed genes in each cluster were identified using the FindAllMarkers function in Seurat. GO enrichment analysis was conducted using Metascape. For pseudotime analysis, the CytoTRACE package was used to determine the relative differentiation state [22]. Monocle2 was used to construct the differentiation trajectory. TSPCs were set as the starting point of differentiation path.

2.21. Statistical analysis

Quantitative data were presented as mean ± standard deviation (SD). Statistical difference between the two groups was assessed using Student's t-test. Multiple group comparisons were assessed using one-way analysis of variance (ANOVA). p values < 0.05 was considered to be statistical significance. * $p < 0.05$, ** $p < 0.01$, *** $p < 0.001$.

3. Results

3.1. Characterization of the biomimetic mineralized collagen hydrogel

To replicate the natural composition of the tendon-bone interface, we developed a bilayer biomimetic collagen hydrogel that encapsulates the transition from non-mineralized to mineralized tissue. The fabrication process of this scaffold initially began with the formation of a collagen hydrogel within a mold, followed by a three-day mineralization phase to form the first layer (Fig. 1A). Then, an additional layer of collagen mixture was carefully applied to the mold to form a second collagen hydrogel layer and ultimately yielding a bilayer biomimetic scaffold (Fig. 1A and B).

Thermogravimetric analysis revealed the incorporation of inorganic components within the mineralized collagen hydrogel, which constituted approximately 30 wt% (Fig. 1C). The nanoindentation tests showed that the elastic modulus was significantly enhanced in the mineralized collagen hydrogel compared to the non-mineralized collagen hydrogel (Fig. 1D). FTIR was used to analyze the chemical composition in both non-mineralized and mineralized samples. Specifically, the amide I, II, and III bands were observed in both non-mineralized and mineralized samples, confirming the characteristic absorption peaks indicative of collagen (Fig. 1E). Furthermore, the mineralized collagen exhibited distinctive peaks that are indicative of the presence of apatitic phosphate (Fig. 1E). Furthermore, TEM and SEM imaging were used to characterize the nanoscale structure. The non-mineralized collagen exhibited a typical banding pattern (Fig. 1F). The mineralized collagen displayed fibrils with partial mineralization, where mineral crystallites were observed both intra- and extrafibrillarly (Fig. 1F). STORM further confirmed intrafibrillar mineralization of collagen (Fig. 1I). Selected area electron diffraction (SAED) analysis of these mineralized fibrils showed characteristic broad arcs corresponding to the (002) and (211) planes, which are consistent with the hexagonal crystal form of hydroxyapatite (Fig. 1F). Cryo-SEM imaging further revealed that both non-mineralized and mineralized collagen possessed a fibrillar structure with porosity (Fig. 1G). Notably, the non-mineralized fibers had a smooth surface, in contrast to the rough surface of mineralized fibers (Fig. S1). EDX profiling of the mineralized specimens confirmed the existence of calcium (Ca) and phosphorus (P) within the matrix (Fig. 1H).

3.2. Biological properties of the biomimetic mineralized collagen hydrogel

In order to engineer the cell-laden collagen hydrogel, cells were encapsulated in the collagen hydrogel and exposed to the mineralization medium or growth medium (Fig. 2A). The live/dead cell staining was employed to evaluate cell viability at 1, 4, and 7 days post-culture, which consistently indicated high biocompatibility of the hydrogel (Fig. 2B). Cells embedded in non-mineralized hydrogel exhibited spindle-shaped morphology, while cells displayed more spread and more filopodia in mineralized hydrogel (Fig. 2C). To explore the effects of mineralization on cell behavior, TSPCs embedded in hydrogels were treated with mineralization medium or growth medium for 3 days. RNA-seq analysis was subsequently conducted to elucidate the comparative gene expression profiles between the two groups. Principal component analysis (PCA) and correlation analysis demonstrated significant differences between these two groups (Fig. 2D and E). Notably, genes associated with osteogenic and chondrogenic differentiation were significantly upregulated in the mineralized group (Fig. 2G). Gene ontology (GO) enrichment analysis of the upregulated genes in mineralized group showed an enrichment of biological processes associated with mineralization and chondrogenesis (Fig. 2H). Overall, these results indicated that biomimetic mineralized collagen could induce the osteochondral differentiation of TSPCs, highlighting the potential of our hydrogel system in mimicking the native tendon-bone interface.

3.3. Evaluation of function and histological recovery

To evaluate the effects of scaffolds on tendon-bone interface repair *in vivo*, a rat model of patella-patellar tendon-interface injury was established (Fig. 3A). Rats were randomly assigned to four groups: BC, NMCH, BMCH, and BMCH-TSPC. Functional recovery is the primary purpose of repair. To evaluate motor ability, rats were tested on a treadmill at 2 and 4 weeks post-surgery. The BMCH-TSPC group showed a significant increase in running distance compared to the NMCH and BC groups at both time points (Fig. 3B). The most notable difference was observed after 4 weeks in comparison to the other three groups (Fig. 3B). At 4 weeks post-surgery, biomechanical assessments were conducted to assess the healing quality of the tendon-bone interface. The biomechanical properties, including stiffness and elastic modulus, were notably enhanced in the BMCH-TSPC group as compared to the BC group (Fig. 3C). Furthermore, the BMCH-TSPC group exhibited significantly higher maximum load and tensile stress compared to both the NMCH and BC groups (Fig. 3C). Taken together, these results demonstrated that BMCH-TSPC effectively promotes enhanced recovery of motor function and mechanical properties after tendon-bone interface injury.

To evaluate the tissue microstructure after recovery, micro-CT and histological analyses were performed. The micro-CT imaging of the patella revealed enhanced new bone regeneration at the tendon-bone interface for both the BMCH-TSPC and BMCH groups, in contrast to the NMCH and BC groups (Fig. 3D). Quantitative analysis confirmed that the bone volume to total volume ratio (BV/TV) was markedly elevated in the BMCH-TSPC group relative to the NMCH and BC groups (Fig. 3E). Furthermore, the CT density within the BMCH-TSPC group was significantly greater than in the other three groups, and the BMCH-TSPC group exhibited the lowest trabecular spacing (Tb.Sp.) (Fig. 3E).

H&E staining and Masson staining revealed reduced fibrovascular tissue, inflammatory cell infiltration, and disorganized fibers and more collagen deposition in the BMCH-TSPC group compared to the NMCH and BC groups (Fig. 4A). In addition, an abundance of chondrocytes was observed in BMCH-TSPC and BMCH groups (Fig. 4A). As expected, the total histologic score of BMCH-TSPC group was the lowest among different groups (Fig. 4C). SO-FG staining and TB staining further substantiated the formation of fibrocartilage in the BMCH-TSPC group, with a significantly larger metachromasia area compared to the other three groups (Fig. 4A and C). Immunofluorescence staining revealed that

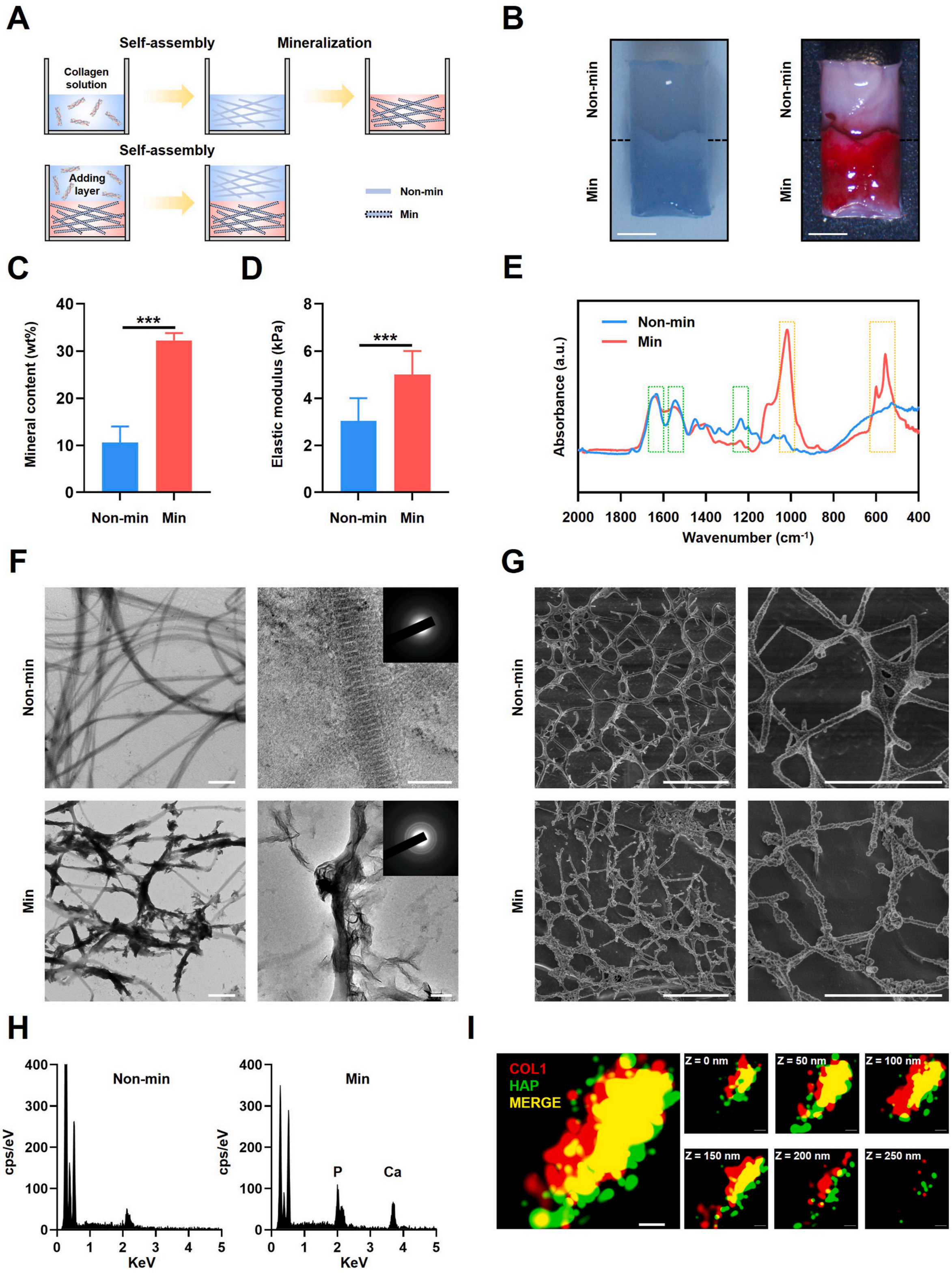

Fig. 1. Fabrication and characterization of the biomimetic hydrogel. (A) Schematic illustration of the biomimetic hydrogel fabrication process. (B) Optical and Alizarin red staining images of the bilayer collagen hydrogel. Scale bar = 1 mm. (C) Thermogravimetric analysis of the mineralized collagen hydrogel and non-mineralized collagen hydrogel. (D) Elastic modulus of the mineralized and non-mineralized collagen hydrogel. (E) FTIR spectra of the mineralized and non-mineralized collagen hydrogels. The green dashed line represented the peak position of amide I, II, and III. The orange dashed line represented the peak position of apatitic phosphate. (F) TEM images and SAED of mineralized and non-mineralized collagen. Scale bar = 1 μm (left), 200 nm (right). (G) Cryo-SEM images of mineralized and non-mineralized collagen. Scale bar = 5 μm (left), 3 μm (right). (H) EDX spectra of mineralized and non-mineralized collagen. (I) STORM image of the mineralized collagen fibrils. Scale bar = 100 nm. Non-min, non-mineralized. Min, mineralized.

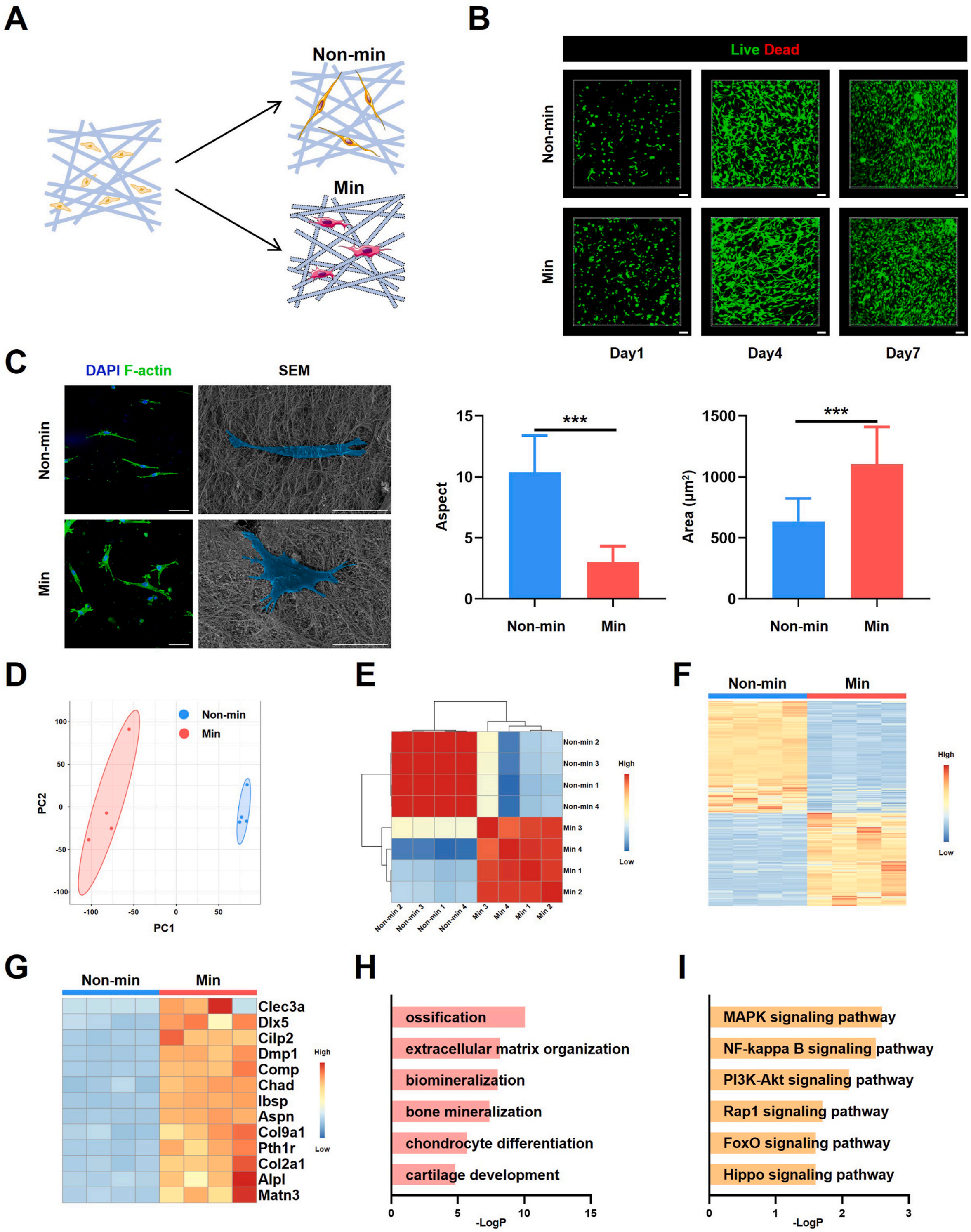

Fig. 2. Analysis of mineralization-induced biological changes. (A) Schematic diagram of cell-laden non-mineralized and mineralized hydrogel. (B) Representative 3D live/dead fluorescence images. Scale bar = 100 μm. (C) Representative fluorescence and SEM images of cell morphology. Aspect and area of F-actin stained cells. Scale bar = 50 μm (fluorescence images), 30 μm (SEM images). (D) PCA plot showing distinct expression patterns. (E) Heatmap showing pearson correlation. (F) Heatmap showing differentially expressed genes between mineralized and non-mineralized group. (G) Heatmap showing the level of gene expression. (H) GO analysis of upregulated genes in mineralized group. (I) KEGG analysis of upregulated genes in mineralized group. Non-min, non-mineralized. Min, mineralized.

increased COL2 and SOX9 expression in the BMCH-TSPC group, further confirming fibrocartilage formation (Fig. 4B). Overall, these results suggested the potent reparative capabilities of BMCH-TSPC, promoting both new bone formation and fibrocartilage regeneration, thereby enhancing the recovery of the tendon-bone interface *in vivo*.

3.4. Analysis of repair effects induced by BMCH-TSPC using single cell transcriptome

To further elucidate the molecular mechanisms driving the regenerative repair process in the BMCH-TSPC group, scRNA-seq was used to

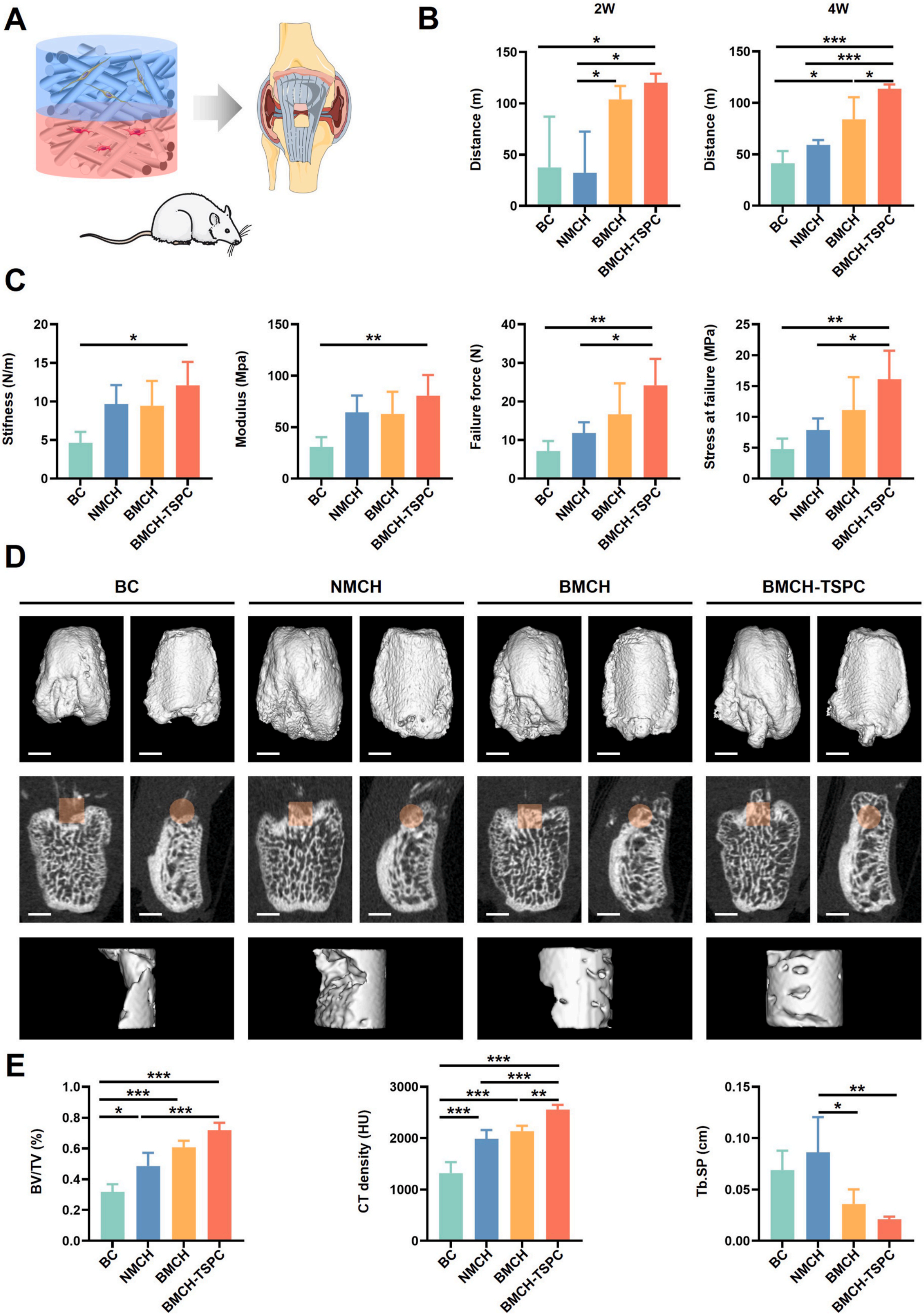

Fig. 3. Cell-laden biomimetic hydrogel promoted functional recovery and new bone formation. (A) Schematic depicts the cell-laden biomimetic hydrogel for tendon-bone interface healing. (B) Running distances of rats at 2 and 4 weeks post-surgery. (C) Biomechanical tests of the repaired interface tissues from different groups at 4 weeks post-surgery. (D) Representative micro-CT images of different groups. Sagittal and coronal-sections, along with 3D reconstruction of micro-CT images, from the specified region of different groups. Scale bar = 1 mm. (E) Quantitative analysis of bone formation in the specified region.

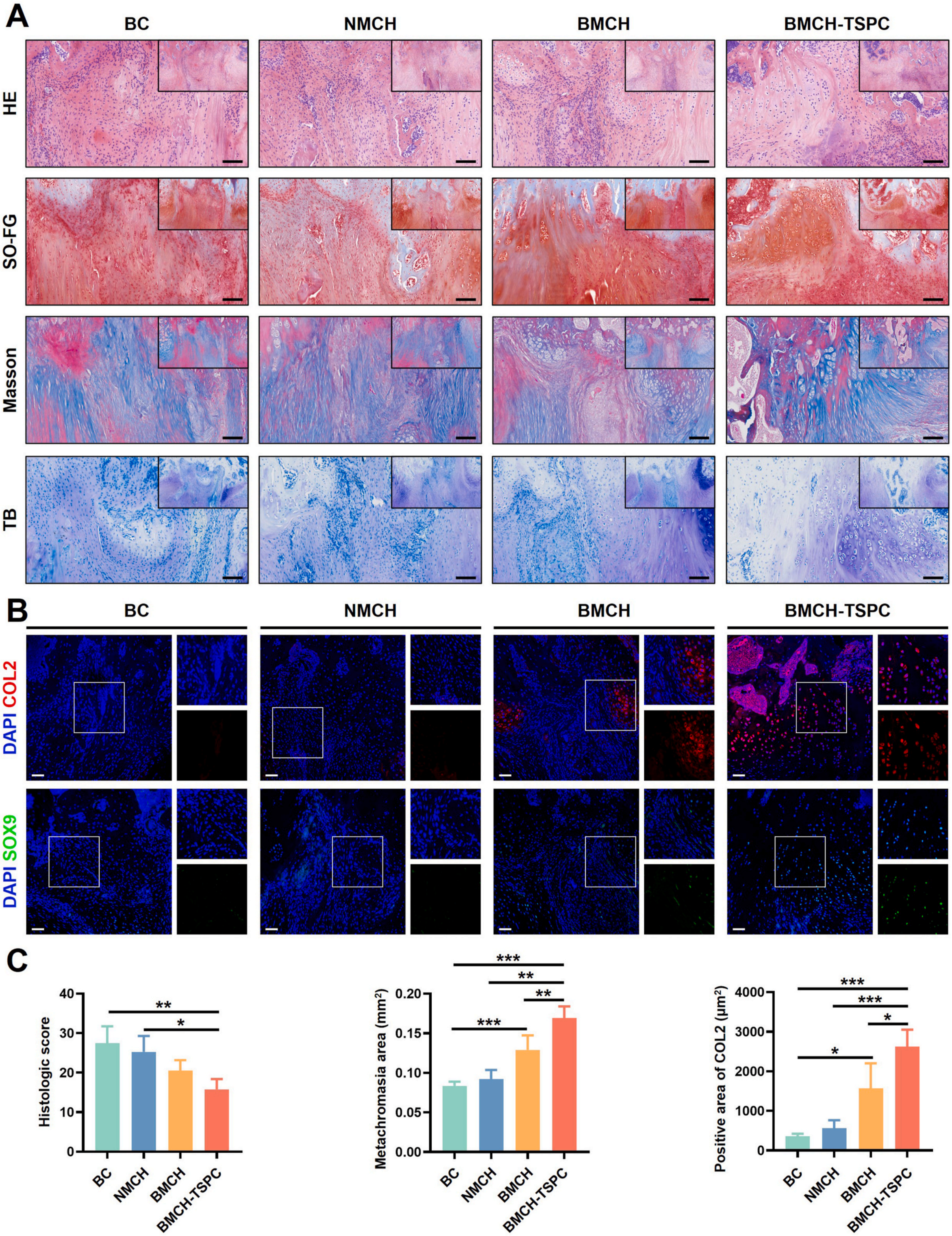

Fig. 4. Cell-laden biomimetic hydrogel promoted histological structure restoration. (A) Representative histological staining images (H&E, SO-FG, TB and Masson) of different groups. Scale bar = 100 μm. (B) Representative immunofluorescence staining images for COL2 and SOX9 of different groups. Scale bar = 50 μm. (C) Histological score, the area of newly formed fibrocartilage, and the area of COL2 of different groups.

delineate the cellular subpopulations after 2 weeks of treatment. Unsupervised clustering identified 13 cell subpopulations, which were defined based on differential expression of markers (Fig. 5A and Fig. S4A). To analyze the tendon-bone cell lineage, the tendon cells and osteochondral cells were further divided into 5 subpopulations (Fig. 5B). TSPCs expressed stem cell markers (such as Thy1, Cd44, and Pdgfra) and were associated with cell migration and regeneration (Fig. 5D and E). CytoTRACE analysis predicted that tendon stem cells were in a less differentiated state (Fig. 5C). Tenoblasts were characterized by classical tendon markers (such as Tnmd, Thbs4, and Postn) and were enriched in extracellular matrix synthesis and response to wounding (Fig. 5D). Fibroblasts expressed Fos, Jun, and Egr1, which are enriched in response

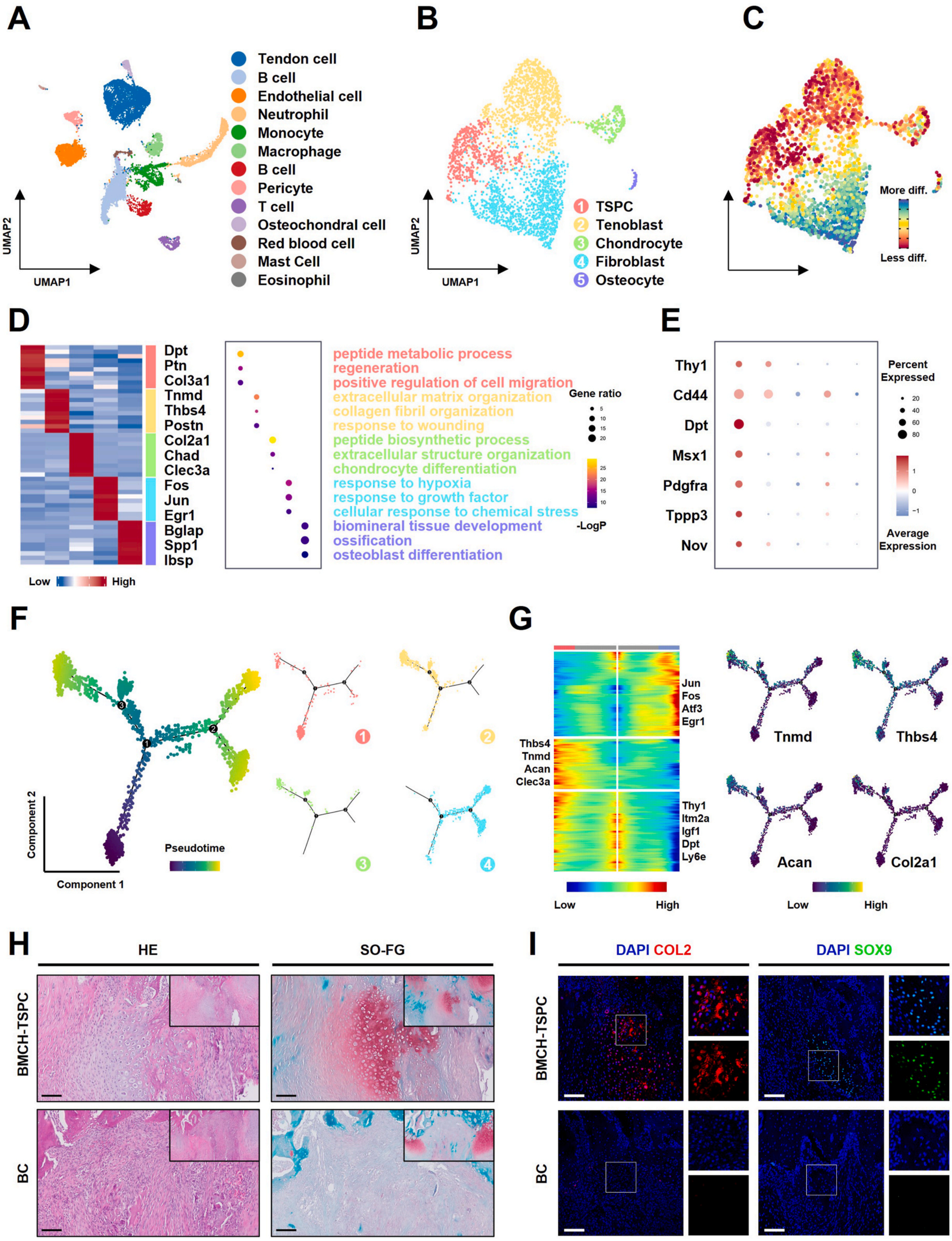

Fig. 5. scRNA-seq analysis of the repaired interface tissues in BMCH-TSPC group. (A) Uniform manifold approximation and projection (UMAP) plot showing the unbiased clustering results. (B) UMAP plot showing the unbiased clustering of tendon-bone cell lineages. (C) Predicted differentiation stages for each cluster. (D) Heatmap showing DEG in each major cluster (left panel). Bubble diagram showing enriched GO terms (right panel). (E) Dotplot showing gene expression levels across clusters. (F) Differentiation trajectory of subpopulations predicted by Monocle2. (G) Heatmap showing gene expressions profiles along the pseudotime of two distinct trajectories (left panel). Expression of genes visualized on differentiation trajectory (right panel). (H) Representative H&E and SO-FG staining images at 2 weeks post-surgery. Scale bar = 100 μm. (I) Representative immunofluorescence staining images for COL2 and SOX9 at 2 weeks post-surgery. Scale bar = 100 μm.

to hypoxia and growth factors (Fig. 5D). Chondrocytes and osteocytes were identified by canonical markers (Fig. 5D).

To explore the lineage relationship among these cell subpopulations, Monocle 2 was used to construct a differentiation trajectory. With tendon stem cells as the starting point, one branch is differentiated to fibroblasts and another to both tendon cells and chondrocytes, with chondrocytes located at the end of the trajectory (Fig. 5F). Genes associated with tendon stem cells, such as Tppp3 and Thy1, were enriched early in the trajectory, while genes indicative of mature tendon (Tnmd, Thbs4) and cartilage (Acan, Col2a1) were found at the pseudotime endpoint (Fig. 5G). Further, the H&E and SO-FG staining showed cartilage formation in the BMCH-TSPC group (Fig. 5H). The COL2 and SOX9 expression was significantly higher in BMCH-TSPC group (Fig. 5I). Taken together, the scRNA-seq analysis provides compelling evidence that tendon stem cells play a pivotal role in the regenerative repair process after tendon-bone injury, highlighting their potential as therapeutic targets for enhancing tendon-bone interface regeneration.

4. Discussion

In this study, we developed a novel stem cell-laden biomimetic hydrogel specifically designed for the repair of the tendon-bone interface. This hydrogel incorporates mineralized collagen fibrils, which exhibited hierarchical mineralization patterns, closely resembling the ultrastructure of the natural tendon-bone interface. Our results showed that this bilayer biomimetic mineralization hydrogel combined with tendon stem cells, effectively promotes fibrocartilage and bone regeneration, thereby accelerating the restoration of both mechanical integrity and motor function, highlighting its promising reparative effects.

Over recent years, significant advancements have been achieved in the development of scaffolds for tendon-bone healing, including decellularized extracellular matrix (ECM) scaffolds and those made from a blend of synthetic or natural materials [6]. Although decellularized ECM scaffolds effectively mimic the natural complex structure, the stringent processing requirements have limited their availability. Based on biomimetic strategies, scaffolds combined with organic synthetic materials, natural materials, and inorganic materials can mimic the composition of the enthesis. However, existing scaffolds failed to replicate the nanoscale characteristics and assembly patterns of the native interface. Lausch et al. developed multiphasic collagen scaffolds, wherein mineralized collagen fibrils have intrafibrillar oriented minerals resembling bone at the nanometer scale [23]. Yet, this study did not assess its regenerative effects *in vivo*. Furthermore, the mineralization solution was unable to construct mineralized scaffolds conducive to cell support. Thrivikraman et al. constructed a cell-laden mineralized hydrogel with both extra and intrafibrillar mineralization, achieved through the supplementation of cell culture media with Ca, P and osteopontin [19]. However, low availability and high cost of natural NCPs limited applications [24]. In our study, we employed cell culture media enriching with Ca, P and pAsp to fabricate mineralized hydrogels, which not only exhibited biomimetic nanostructure but also significantly promoted tendon-bone repair.

Stem cells play a pivotal role in tissue regeneration. As tendon-bone tissue matures, the number of stem/progenitor cells gradually decreases [25,26]. Exogenous supplementation of stem cells has been shown to promote tissue regeneration. For example, Du et al. fabricated bilayered biomimetic multicellular scaffolds containing TSPCs and BMSCs using 3D printing, which significantly improved fibrocartilage regeneration and the recovery of mechanical properties in a rotator cuff tear model compared to cell-free scaffolds [27]. Our study is consistent with these findings, as biomimetic scaffolds seeded with TSPCs showed superior repair effect compared to their cell-free counterparts, indicating the pivotal role of tendon stem cells in promoting tendon-bone repair. Tissue regeneration and repair involve diverse cell types. scRNA-seq analysis provides a deeper understanding of the cellular landscape and biological processes during tissue repair [28]. For example, Zhang et al. conducted scRNA-seq analysis, and found that neurotrophic supplements-incorporated 3D-printed hydrogels led to an expansion of the resident Msx1+ skeletal stem cells, thereby promoting bone regeneration [29]. In this study, we used scRNA-seq to resolve cellular subpopulations involved in tendon-bone repair and traced the differentiation trajectory of TSPCs into chondrocytes, indicating their involvement in the tendon-bone regeneration process. However, our study did not address the *in vivo* fate of TSPCs. Future research utilizing single-cell lineage tracing techniques is expected to provide further insights into the role of these cells during the tendon-bone repair process.

In summary, we developed an *in vitro* tendon-bone-like construct that mimics the nanoscale structure of natural tendon-bone interface. This biomimetic construct presents a promising approach for tendon-bone interface healing.

CRediT authorship contribution statement

Tingyun Lei: Writing – original draft, Visualization, Methodology, Investigation, Data curation, Conceptualization. **Tao Zhang:** Methodology, Investigation. **Tianshun Fang:** Investigation. **Jie Han:** Investigation. **Chunyi Gu:** Investigation. **Youguo Liao:** Investigation. **Yang Fei:** Investigation. **Junchao Luo:** Investigation. **Huanhuan Liu:** Writing – review & editing. **Yan Wu:** Funding acquisition. **Weiliang Shen:** Resources, Supervision. **Xiao Chen:** Writing – review & editing, Supervision, Resources, Funding acquisition, Conceptualization. **Zi Yin:** Writing – review & editing, Supervision, Resources, Funding acquisition, Conceptualization. **Junjuan Wang:** Writing – review & editing, Supervision, Methodology, Investigation, Data curation, Conceptualization.

Ethics approval and consent to participate

All animal experiments were approved by Institutional Animal Care and Use Committee of Zhejiang University (ZJU20230256).

Declaration of competing interest

The authors declare that they have no known competing financial interests or personal relationships that could have appeared to influence the work reported in this paper.

Acknowledgement

This work was supported by the National key research and development program of China (2022YFA1106800), NSFC grants (82222044, T2121004, 32271404), Key R&D Program of Zhejiang (2024SSYS0026), “Leading Goose” Science and Technology Project of Zhejiang Province (2023C03093), Zhejiang Provincial Natural Science Foundation of China (LZ22H060002).

We thank Shuangshuang Liu, Wei Yin and Jingyao Chen from the Core Facilities, Zhejiang University School of Medicine for their technical support. We thank Guizhen Zhu and Dandan Song in the Center of Cryo-Electron Microscopy (CCEM), Zhejiang University for her technical assistance on scanning electron microscopy. We thank Xiaomin Zhang and Li Xie from the Analysis Center of Agrobiology and Environment Sciences of Zhejiang University for their technical assistance.

Appendix A. Supplementary data

Supplementary data to this article can be found online at https://doi.org/10.1016/j.bioactmat.2025.03.001.

References

[1] M. Golman, A.C. Abraham, I. Kurtaliaj, B.P. Marshall, Y.J. Hu, A.G. Schwartz, X. E. Guo, V. Birman, P.J. Thurner, G.M. Genin, S. Thomopoulos, Toughening mechanisms for the attachment of architectured materials: the mechanics of the

tendon enthesis, Sci. Adv. 7 (2021), https://doi.org/10.1126/sciadv.abi5584 eabi5584.

[2] S. Font Tellado, E.R. Balmayor, M. Van Griensven, Strategies to engineer tendon/ligament-to-bone interface: biomaterials, cells and growth factors, Adv. Drug Deliv. Rev. 94 (2015) 126–140, https://doi.org/10.1016/j.addr.2015.03.004.

[3] A. Bedi, J. Bishop, J. Keener, D.A. Lansdown, O. Levy, P. MacDonald, N. Maffulli, J. H. Oh, V.J. Sabesan, J. Sanchez-Sotelo, R.J. Williams, B.T. Feeley, Rotator cuff tears, Nat. Rev. Dis. Primers 10 (2024), https://doi.org/10.1038/s41572-024-00492-3.

[4] Q. Shengnan, S. Bennett, W. Wen, L. Aiguo, X. Jiake, The role of tendon derived stem/progenitor cells and extracellular matrix components in the bone tendon junction repair, Bone 153 (2021) 116172, https://doi.org/10.1016/j.bone.2021.116172.

[5] S. Zhao, W. Su, V. Shah, D. Hobson, L. Yildirimer, K.W.K. Yeung, J. Zhao, W. Cui, X. Zhao, Biomaterials based strategies for rotator cuff repair, Colloids Surf. B Biointerfaces 157 (2017) 407–416, https://doi.org/10.1016/j.colsurfb.2017.06.004.

[6] T. Lei, T. Zhang, W. Ju, X. Chen, B.C. Heng, W. Shen, Z. Yin, Biomimetic strategies for tendon/ligament-to-bone interface regeneration, Bioact. Mater. 6 (2021) 2491–2510, https://doi.org/10.1016/j.bioactmat.2021.01.022.

[7] N. Reznikov, M. Bilton, L. Lari, M.M. Stevens, R. Kröger, Fractal-like hierarchical organization of bone begins at the nanoscale, Science 360 (2018), https://doi.org/10.1126/science.aao2189.

[8] T. Zhang, T. Lei, J. Han, R. Zhang, W. Shen, Y. Liu, Y. Liao, Y. Zhao, X. Zhang, R. Yan, Q. He, Y. Chen, H. Pan, H. Ouyang, L. Wang, W. Yin, Z. Yin, X. Chen, Bio-inspired mineralization collagen induce fibrocartilage regeneration after tendon-bone injury by activating gli1+dkk3+ progenitor cells, bioRxiv (2023), https://doi.org/10.1101/2023.09.24.557863.

[9] D.J. Buss, K. Rechav, N. Reznikov, M.D. McKee, Mineral tessellation in mouse enthesis fibrocartilage, achilles tendon, and hyp calcifying enthesopathy: a shared 3d mineralization pattern, Bone 174 (2023) 116818, https://doi.org/10.1016/j.bone.2023.116818.

[10] S. Zhang, W. Ju, X. Chen, Y. Zhao, L. Feng, Z. Yin, X. Chen, Hierarchical ultrastructure: an overview of what is known about tendons and future perspective for tendon engineering, Bioact. Mater. 8 (2022) 124–139, https://doi.org/10.1016/j.bioactmat.2021.06.007.

[11] J. Mahamid, A. Sharir, L. Addadi, S. Weiner, Amorphous calcium phosphate is a major component of the forming fin bones of zebrafish: indications for an amorphous precursor phase, Proc. National Academy of Sci. PNAS 105 (2008) 12748–12753, https://doi.org/10.1073/pnas.0803354105.

[12] J. Mahamid, B. Aichmayer, E. Shimoni, R. Ziblat, C. Li, S. Siegel, O. Paris, P. Fratzl, S. Weiner, L. Addadi, Mapping amorphous calcium phosphate transformation into crystalline mineral from the cell to the bone in zebrafish fin rays, Proc. Natl. Acad. Sci. USA 107 (2010) 6316–6321, https://doi.org/10.1073/pnas.0914218107.

[13] S. Boonrungsiman, E. Gentleman, R. Carzaniga, N.D. Evans, D.W. McComb, A. E. Porter, M.M. Stevens, The role of intracellular calcium phosphate in osteoblast-mediated bone apatite formation, Proc. Natl. Acad. Sci. USA 109 (2012) 14170–14175, https://doi.org/10.1073/pnas.1208916109.

[14] Z. Xu, W. Zhao, Z. Wang, Y. Yang, N. Sahai, Structure analysis of collagen fibril at atomic-level resolution and its implications for intra-fibrillar transport in bone biomineralization, Phys. Chem. Chem. Phys. : Phys. Chem. Chem. Phys. 2 (2018) 1513–1523, https://doi.org/10.1039/c7cp05261h.

[15] S. Shan, Z. Tang, K. Sun, W. Jin, H. Pan, R. Tang, W. Yin, Z. Xie, Z. Chen, C. Shao, ACP-mediated phase transformation for collagen mineralization: a new understanding of the mechanism, Adv. Healthcare Mater. 13 (2024), https://doi.org/10.1002/adhm.202302418.

[16] F. Nudelman, K. Pieterse, A. George, P.H. Bomans, H. Friedrich, L.J. Brylka, P. A. Hilbers, G. de With, N.A. Sommerdijk, The role of collagen in bone apatite formation in the presence of hydroxyapatite nucleation inhibitors, Nat. Mater. 9 (2010) 1004–1009, https://doi.org/10.1038/nmat2875.

[17] B.M. Oosterlaken, M.P. Vena, G. With, In vitro mineralization of collagen, Adv. Mater. 33 (2021) 2004418, https://doi.org/10.1002/adma.202004418.

[18] Z. Liu, M. Tang, J. Zhao, R. Chai, J. Kang, Looking into the future: toward advanced 3d biomaterials for stem-cell-based regenerative medicine, Adv. Mater. 30 (2018), https://doi.org/10.1002/adma.201705388.

[19] G. Thrivikraman, A. Athirasala, R. Gordon, L. Zhang, R. Bergan, D.R. Keene, J. M. Jones, H. Xie, Z. Chen, J. Tao, B. Wingender, L. Gower, J.L. Ferracane, L. E. Bertassoni, Rapid fabrication of vascularized and innervated cell-laden bone models with biomimetic intrafibrillar collagen mineralization, Nat. Commun. 10 (2019), https://doi.org/10.1038/s41467-019-11455-8.

[20] S. Qin, W. Wang, Z. Liu, X. Hua, S. Fu, F. Dong, A. Li, Z. Liu, P. Wang, L. Dai, P. Liang, J. Zhang, W. Cao, X. Xiong, H. Chen, J. Xu, Fibrochondrogenic differentiation potential of tendon-derived stem/progenitor cells from human patellar tendon, J. Orthop. Transl. 22 (2020) 101–108, https://doi.org/10.1016/j.jot.2019.08.006.

[21] Z. Wang, C. Ma, D. Chen, C. Haslett, C. Xu, C. Dong, X. Wang, M. Zheng, Y. Jing, J. Q. Feng, Tendon cells root into (instead of attach to) humeral bone head via fibrocartilage-enthesis, Int. J. Biol. Sci. 19 (2023) 183–203, https://doi.org/10.7150/ijbs.79007.

[22] G.S. Gulati, S.S. Sikandar, D.J. Wesche, A. Manjunath, A. Bharadwaj, M.J. Berger, F. Ilagan, A.H. Kuo, R.W. Hsieh, S. Cai, M. Zabala, F.A. Scheeren, N.A. Lobo, D. Qian, F.B. Yu, F.M. Dirbas, M.F. Clarke, A.M. Newman, Single-cell transcriptional diversity is a hallmark of developmental potential, Science 367 (2020) 405–411, https://doi.org/10.1126/science.aax0249.

[23] A.J. Lausch, L.C. Chong, H. Uludag, E.D. Sone, Multiphasic collagen scaffolds for engineered tissue interfaces, Adv. Funct. Mater. 28 (2018) 1804730, https://doi.org/10.1002/adfm.201804730.

[24] L. Yu, M. Wei, Biomineralization of collagen-based materials for hard tissue repair, Int. J. Mol. Sci. 22 (2021) 944, https://doi.org/10.3390/ijms22020944.

[25] A.G. Schwartz, L.M. Galatz, S. Thomopoulos, Enthesis regeneration: a role for gli1 + progenitor cells, Development 144 (2017) 1159–1164, https://doi.org/10.1242/dev.139303.

[26] K. Ideo, T. Tokunaga, C. Shukunami, A. Takimoto, Y. Yoshimoto, R. Yonemitsu, T. Karasugi, H. Mizuta, Y. Hiraki, T. Miyamoto, Role of scx+/sox9+ cells as potential progenitor cells for postnatal supraspinatus enthesis formation and healing after injury in mice, PLoS One 15 (2020) e0242286, https://doi.org/10.1371/journal.pone.0242286.

[27] L. Du, C. Qin, H. Zhang, F. Han, J. Xue, Y. Wang, J. Wu, Y. Xiao, Z. Huan, C. Wu, Multicellular bioprinting of biomimetic inks for tendon-to-bone regeneration, Adv. Sci. 10 (2023), https://doi.org/10.1002/advs.202301309.

[28] A. Ruta, K. Krishnan, J.H. Elisseeff, Single-cell transcriptomics in tissue engineering and regenerative medicine, Nature Reviews Bioeng. 2 (2024) 101–119, https://doi.org/10.1038/s44222-023-00132-7.

[29] X. Zhang, W. Jiang, C. Xie, X. Wu, Q. Ren, F. Wang, X. Shen, Y. Hong, H. Wu, Y. Liao, Y. Zhang, R. Liang, W. Sun, Y. Gu, T. Zhang, Y. Chen, W. Wei, S. Zhang, W. Zou, H. Ouyang, Msx1+ stem cells recruited by bioactive tissue engineering graft for bone regeneration, Nat. Commun. 13 (2022), https://doi.org/10.1038/s41467-022-32868-y.